Journal of Magnetic Resonance Open 18 (2024) 100144

Contents lists available at ScienceDirect

Journal of Magnetic Resonance Open

journal homepage: www.sciencedirect.com/journal/journal-of-magnetic-resonance-open

Research article

Polarization losses from the nonadiabatic passage of hyperpolarized solutions through metallic components

James Eills [a], Marc Azagra [a], David Gómez-Cabeza [a], Michael C.D. Tayler [b], Irene Marco-Rius [a,*]

[a] IBEC - Institute for Bioengineering of Catalonia, Barcelona Institute of Science and Technology, 08028 Barcelona, Spain
[b] ICFO - Institut de Ciències Fotòniques, The Barcelona Institute of Science and Technology, 08860 Castelldefels, Barcelona, Spain

ARTICLE INFO

Keywords:
Hyperpolarization
Non-adiabatic
Low-field MRI
Spin relaxation
Benchtop NMR

ABSTRACT

From complex-mixture analysis to in vivo molecular imaging, applications of liquid-state nuclear spin hyperpolarization have expanded widely over recent years. In most cases, hyperpolarized solutions are generated ex situ and transported from the polarization instrument to the measurement device. The sample hyperpolarization usually survives this transport, since the changes in magnetic fields that are external to the sample are typically adiabatic (slow) with respect to the internal nuclear spin dynamics. The passage of polarized samples through weakly magnetic components such as stainless steel syringe needles and ferrules is not always adiabatic, which can lead to near-complete destruction of the magnetization. To avoid this effect becoming "folklore" in the field of hyperpolarized NMR, we present a systematic investigation to highlight the problem and investigate possible solutions. Experiments were carried out on: (i) dissolution-DNP-polarized [1-^{13}C]pyruvate with NMR detection at 1.4 T, and (ii) 1.5-T-polarized H_2O with NMR detection at 2.5 μT. We show that the degree of adiabaticity of solutions passing through metal parts is intrinsically unpredictable, likely depending on many factors such as solution flow rate, degree of remanent ferromagnetism in the metal, and nuclear spin species. However, the magnetization destruction effects can be suppressed by application of an external field on the order of 0.1–10 mT.

1. Introduction

Hyperpolarization methods such as dissolution dynamic nuclear polarization (dDNP) [1–5] and parahydrogen-induced polarization (PHIP) [6–10] are used to enhance the polarization of a nuclear spin ensemble far beyond the thermal equilibrium level. This can lead to signal enhancements of molecules in the liquid state on the order of 10^4 to 10^5 compared to polarization in a high-field (e.g., 1–10 T) NMR magnet [11]. This remarkable increase in signal strength has opened the door to many applications such as in vivo metabolic imaging, [12–16] the elucidation of biomolecular structures, [17–20] investigations of polymers and viscous liquids [21,22] plus heterogeneous and homogeneous hydrogenation reaction mechanisms, [23–26] and many more. Central to most of these applications is that the nuclear spin polarization survives movement of the liquid sample, for example during transport across a laboratory, or during sample mixing, because the hyperpolarization procedure is often carried out away from the measurement device in a separate instrument [27].

The profile of magnetic field experienced by the sample vs. time determines the survival of nuclear spin polarization during transport. On the one hand, spin relaxation governs how rapidly polarization returns to thermal equilibrium and is generally (although not always) characterized by a decay time constant, T_1, that is field-dependent. Generally, if the transport time is similar to or longer than T_1, a significant fraction (more than half) of the starting polarization is lost. On the other hand, and relevant to this work, is the rate of change in orientation of the background magnetic field: spin polarization can be lost if the external magnetic field is rotated sufficiently rapidly such that the nuclear spins do not have time to reorient to follow the change.

It can be estimated that to maintain adiabaticity, the rate of rotation of the external field (ω_{rot}) should be lower than the rate of nuclear spin precession ω_0 in the field [28]. In Fig. 1 we show this principle for a spin-1/2 nucleus of gyromagnetic ratio γ: the nucleus is initially aligned in a magnetic field along the x axis. The magnetic field is then reoriented to the y axis at a constant angular rate, $\omega_{rot} = d\phi/dt$, and then held static along y. We show a simulation of the nuclear spin trajectory for seven different rates of rotation, which are given as a fraction of the nuclear spin Larmor frequency in the field ($\omega_0 = \gamma B_0$). It can be seen that when ω_{rot} is more than 10× lower than ω, the spin follows the field change approximately adiabatically.

The earth's field is in principle sufficiently strong and homogeneous to satisfy adiabaticity, even at high transport rates such as fluid flow

* Corresponding author.
E-mail address: imarco@ibecbarcelona.eu (I. Marco-Rius).

https://doi.org/10.1016/j.jmro.2023.100144
Received 30 September 2023; Received in revised form 21 December 2023; Accepted 23 December 2023
Available online 12 January 2024

inside capillary tubes [29–36]. However, in an unshielded laboratory environment there exist additional background fields from magnetic objects, such as NMR magnets or electrical laboratory equipment. In this case, the total magnetic field is much less homogeneous, and may be weak enough so that adiabaticity cannot be fulfilled when the sample is in motion. These points in space are colloquially referred to as a 'zero-field crossings' [37]. This term is helpful, although it may be slightly misleading since it is likely that inhomogeneity in the directionality of the field lines (causing an effective rotation in the B_0 field during transport) is more problematic than going to low field itself.

One way to maintain adiabaticity in order to preserve spin polarization is to provide a high magnetic field along the sample transport path by using a magnetic tunnel [31,37–39]. This is particularly helpful for solid samples where strong intermolecular dipole–dipole couplings can lead to nonadiabatic transfer effects near Earth's field, because these couplings become the interaction of leading strength [40]. An additional benefit of magnetic tunnels is that T_1 time constants are often slightly longer in elevated field compared to Earth's field, [41,42] especially if the solution contains paramagnetic species such as the radicals used for the DNP process or quadrupolar nuclei, such as ^{14}N [43].

We have observed in experiments with hyperpolarized samples that passage of the sample through stainless steel parts such as syringe needles or through capillary tubing supporting nuts/ferrules can lead to partial or complete loss of the hyperpolarization. We attribute this to the spins experiencing nonadiabatic changes in the B_0 field when passing rapidly through these small-diameter, weakly ferromagnetic parts. In this work we investigate how nuclear spin polarization in liquid samples is affected by passage through stainless steel syringe needles under conditions such as the needle length/diameter, orientation in space with respect to the ambient field, and strength of additional guiding fields. We have carried out experiments with dDNP-polarized [1-^{13}C]pyruvate detected in a 1.4 T bench-top NMR magnet, and with water polarized in a 1 T permanent magnet, detected in a sub-Earth's-field spectrometer.

2. Results

2.1. High-field experiments with hyperpolarized [1-^{13}C]pyruvate

A concentrated pellet of neat [1-^{13}C]pyruvic acid was polarized via dissolution DNP using a HyperSense polarizer (Oxford Instruments, U.K.), and ejected via rapid dissolution. The resulting pH neutral solution contained [1-^{13}C]pyruvate at 80 mM concentration and 12% ^{13}C polarization. 4 mL of this solution were immediately diluted further with distilled H_2O to bring the total volume up to 20 mL. Then, 400 μL aliquots of this solution were dispensed sequentially into a series of 5 mm o.d. NMR tubes using either a plastic capillary or a syringe needle to direct the solution into each tube. These dispensing operations were performed rapidly (one every few seconds), and the tubes were taken every 10 s for signal acquisition. An illustration of the experiment is shown in Fig. 2(a,b). Initial NMR acquisitions on NMR tubes filled via a PEEK capillary served as control points, since the hyperpolarized solutions did not come into contact with any metal parts. Subsequent NMR tubes were filled using seven different metal syringe needles, as shown in Table 1 (in the Materials and Methods) and Fig. 2(c). The solution was either supplied through the needle in Earth's field (cyan), with a neodymium N52 bar magnet (1.45 T remanent field) held next to the needle (purple), or with the needle inside a 1 T Halbach magnet (gold). The resulting data are shown in Fig. 2(e).

We observe that the control spectra (black points) in Fig. 2 show an exponential decay in amplitude over time, with a time constant of 56 ± 0.4 s. This corresponds to the ^{13}C T_1 decay time constant of the solutions in Earth's field, during the period when the samples were kept outside the NMR magnet prior to measurement. Injection

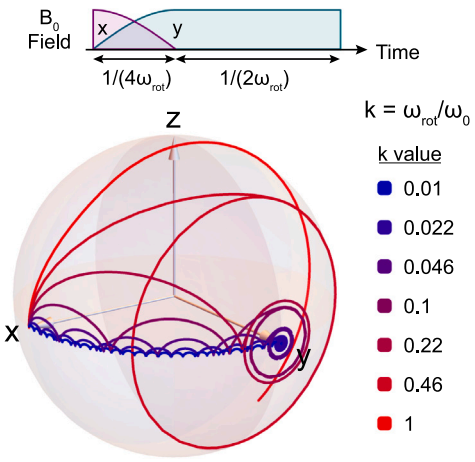

Fig. 1. Nuclear magnetization trajectories under an x→y ($\phi = 0 \rightarrow \pi/2$) background magnetic field reorientation at a constant rate $\omega_{rot} = d\phi/dt = k\gamma B_0$, where ϕ is the azimuthal angle of the magnetic field, and k is a constant of proportionality. The field rotation frequencies are given as a fraction of the nuclear spin Larmor frequency (ω_0, where $\omega_0 = \gamma B_0$) in the B_0 field (which is a constant since B_0 is fixed in amplitude and only changes in direction). The nuclear spin is initially aligned along x, and after a $\pi/2$ field rotation from x→y, the field is held static along y for a short period. It can be seen that the nuclear spin follows the field rotation mostly adiabatically when ω_{rot} is about 10× lower than the Larmor frequency (i.e., $k = 0.1$), but becomes nonadiabatic for faster rotations.

through a syringe needle reduced the magnitude of the NMR signal by at least a factor of 10 in almost all cases, with the exception of needles II and III. In one case (needle VI) the resulting ^{13}C signal was still weakly hyperpolarized but inverted in sign, indicating that (as expected) these signal losses result from nonadiabatic passage through the needle and not an incoherent relaxation process. In contrast, when the N52 permanent magnet was placed adjacent to the needle during injection, and likewise when the needle was placed inside a permanent 1 T Halbach magnet, the polarization was preserved in all cases.

In Fig. 2(d) a comparison between ^{13}C spectra in the frequency range of the pyruvate C1 site is shown for a sample injected through a plastic capillary and through syringe needle I. For the solution that passed through the syringe needle, the central peak at 172 ppm is almost completely lost. The additional peaks in the spectrum, which somewhat survive, are ^{13}C satellite peaks from the [1,2-$^{13}C_2$] (outer satellites) and [1,3-$^{13}C_2$] (inner satellites) pyruvate isotopologs.

To understand whether the alignment of the needle in space (i.e., its alignment in the laboratory magnetic field) affects the adiabaticity of the process, we repeated the multi-injection experiment, with the hyperpolarized solution delivered to the NMR tubes through different orientations of the needle VII in space (Fig. 3(a)). We also performed periodic control experiments, injecting the pyruvate solution through a plastic capillary into the NMR tubes. As before, the NMR tubes were placed in a 1.4 T bench-top NMR spectrometer for ^{13}C signal acquisition, and the integrals of the C1 [1-^{13}C]pyruvate NMR signals are plotted in Fig. 3(c). The orientation of the needle with respect to the axis system of the laboratory is denoted in spherical coordinates as (θ, ϕ), with θ the polar angle and ϕ the azimuthal angle, next to the corresponding data point. These data indicate that the orientation of the needle in space does not significantly influence the dephasing of the spins, since in all cases a signal reduction by more than a factor of 10 is observed.

We then carried out an experiment to determine what strength of applied magnetic field around the syringe needle would make the injection process adiabatic to preserve the ^{13}C hyperpolarization. The hyperpolarized [1-^{13}C]pyruvate multi-injection experiment was repeated using needle VII, with a solenoid electromagnet wrapped around the needle to provide a guiding magnetic field (Fig. 3(b)). The strength

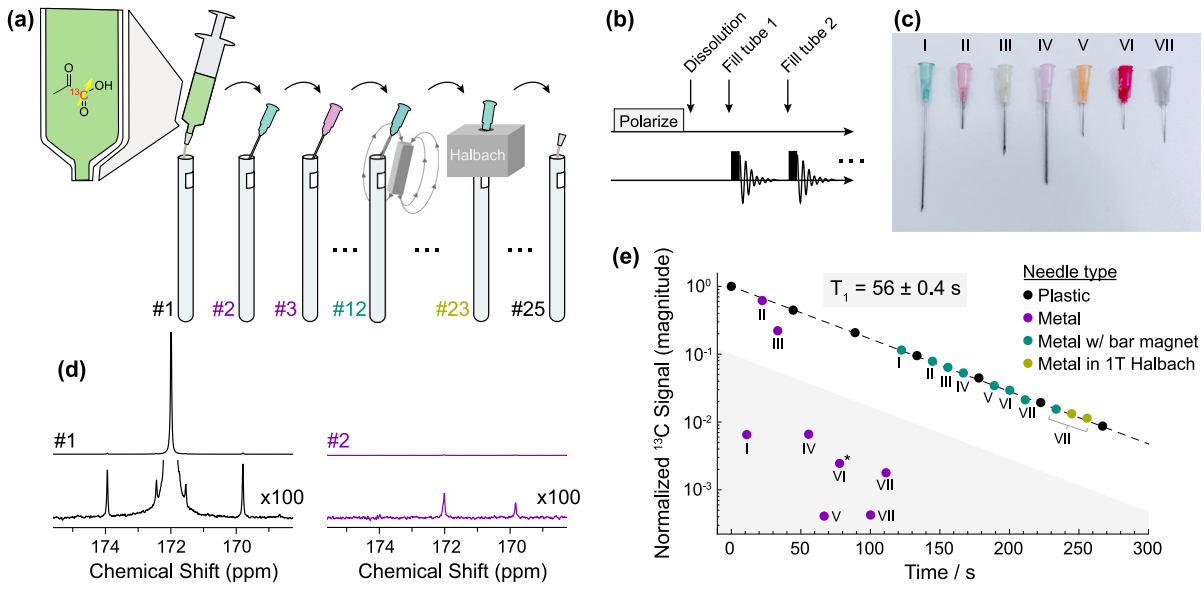

Fig. 2. (a) Experimental schematic illustrating the methodological progression: initial NMR tube filling via a PEEK capillary for the first acquisition is indicated by #1. Subsequent NMR tubes were filled using individual syringe needles for acquisitions #2-#25, with strategic positioning of an N52 bar magnet for acquisitions #12-#22 or a 1T Halbach magnet for acquisitions #23-#25. (b) Simplified sequence showing the experimental procedure. (c) The 7 syringe needles used for this experiment. (d) A comparison between the ^{1}H-decoupled ^{13}C NMR spectra of acquisitions #1 (left) and #2 (right) illustrated in (a), showing a significant decrease of the [1-^{13}C]pyruvate ^{13}C signal when the sample was passed through a syringe needle in (#2). The bottom spectra are a vertical zoom ×100 of the corresponding top spectra. The satellite peaks observed are from the natural abundance of pyruvate molecules with an additional ^{13}C nucleus in the C2 or C3 position. (e) Effect of different injection conditions on [1-^{13}C]pyruvate liquid-state polarization. Data points represent the integrals (absolute value) of the [1-^{13}C]pyruvate ^{13}C NMR signal of the labelled C1 position, normalized to 1 for the first scan. The dotted line represents an exponential decay function of the form $M(t) = M_0 \exp(-t/T_1)$ fit to the data, and the fitted T_1 value is given in the plot. The grey shaded region represents the area in which the ^{13}C integral is more than 10× lower than predicted from the control experiments. The asterisk denotes a data point with negative amplitude.

of the guiding field was varied between experiments by changing the current through the coil with a variable DC power supply. The ^{13}C NMR signal integrals from the C1 site in [1-^{13}C]pyruvate are shown in Fig. 3(d). The applied field for each injection is shown next to the corresponding data point. We observed that a field of between 3.25 mT and 6.5 mT was required for the solution transport through the needle to be adiabatic.

Periodically, for some experiments in this series, the pyruvate solution was injected through the plastic capillary to obtain reference signals to quantify the polarization loss. In Fig. 4 we show a comparison between the ^{13}C spectra for two hyperpolarized [1-^{13}C]pyruvate samples: one that passed through a plastic capillary and the other that passed through needle VII. For the latter, the central peak from the C1 site is dramatically reduced in amplitude by the nonadiabatic passage through the needle, but the carbon satellite peaks from the 1.1% of molecules with a ^{13}C nucleus in the C2 position remain hyperpolarized. The ^{13}C NMR signal of the C2 carbon (207 ppm) is also mostly unaffected by the needle passage. The chemical shift difference between the two carbon sites is 35.1 ppm and the $^{1}J_{CC}$-coupling is 62 Hz, meaning the J-coupling dominates at low fields, leading to a change in the eigenbasis to the singlet–triplet basis. The ^{13}C-^{13}C singlet state is a nonmagnetic state that is unaffected by the magnetic field changes experienced during sample transport (i.e., from the needle passage), but is transformed back into an observable magnetic state as the sample is placed in the high-field NMR magnet. Our observation is the same effect as reported in Refs. [31,44–46], although in our work the samples were not ^{13}C-enriched so we only observe the effect for the 1.1% of molecules with a ^{13}C spin in the C2 position.

To better understand this, we can assume the DNP process generates an excess of population in the $\alpha\alpha$ state which leads to over-population of the T_+ state at low field. For a sample that does not pass through the needle, relaxation leads to partial redistribution of the spin population within the triplet manifold, but a strong singlet-triplet imbalance remains because triplet-to-singlet transitions are nominally forbidden by symmetry rules, and immune to many relaxation mechanisms [45,47,48]. For a sample that does pass through the syringe needle, this process leads to destruction of magnetization which we model as equalization of the three triplet state populations, but this process cannot induce triplet ↔ singlet transitions so the S_0 state remains depleted. Upon adiabatic return to high field, both samples exhibit hyperpolarized NMR signals due to the singlet-triplet population imbalance. The spin state populations and eigenbasis changes throughout this process are depicted in Fig. 4.

We additionally investigated the magnetization-loss effect for hyperpolarized [1-^{13}C]pyruvate samples passing through stainless steel ferrules and nuts, which are common components of the connections used in fluidic transport lines. The hyperpolarized sample was collected in a syringe and injected into a series of NMR tubes through one of three capillary tubes, where the tube passes through: (1) no metallic parts (control), (2) a 1/16" ferrule, and (3) a ferrule+nut set (1/16" i.d., 10–32 threads). The capillary in all cases was a 1/16" O.D., 1/32" I.D. polyether ether ketone tube (Part No. 211608, BGB Analytik). The results from this experiment and a diagram showing the three capillaries used are shown in Fig. 5. As expected, passage of the sample through the metal components does cause polarization losses, although the effect is significantly weaker than for metal syringe needles. The typical signal reduction (compared to the control experiment) was 30 ± 10% and 50 ± 20%, respectively. Although these polarization losses are relatively minor compared to the near-complete loss observed from passage through metal needles and indeed may go unnoticed, they nonetheless cause some concern. For example, in metabolic tracing applications a minor inconsistency in the NMR signal as introduced by the losses may be comparable to the variation caused by other parameters, leading to false conclusions.

2.2. Low-field experiments with magnetized water

A further systematic study of nuclear magnetization loss during passage through metal was made without using hyperpolarized ^{13}C. A gravity-driven, continuous-flow fluid path like the one illustrated

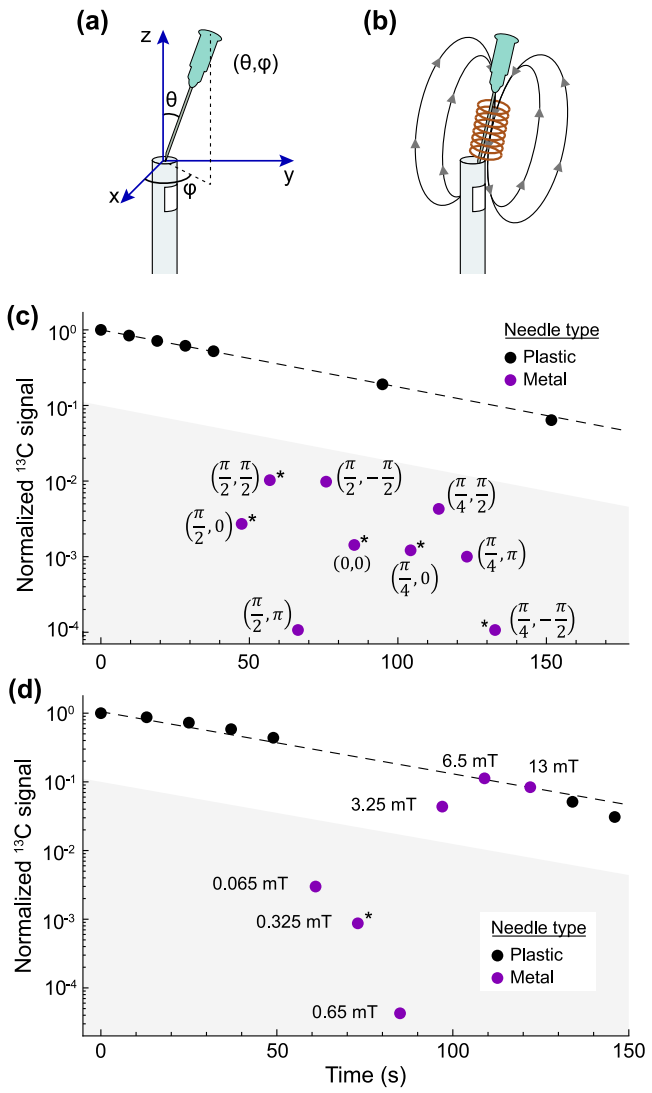

Fig. 3. (a,c) Effect of the angle of the syringe needle in space on the ^{13}C polarization. Data points represent the integrals (absolute value) of the [1-^{13}C]pyruvate ^{13}C NMR signal of the labelled C1 position, normalized to 1 for the first scan. Numbers in brackets represent the angle of the needle with respect to the laboratory in spherical coordinates, as represented in part (a). The dotted line represents an exponential decay function fit to the data, and the grey shaded region represents the area in which the ^{13}C integral is more than an order of magnitude lower than predicted from the control experiments. Asterisks indicate data points that have a negative integral. (b,d) Effect of an applied magnetic field on the ^{13}C polarization. The experiment was carried out with the needles always upright in an NMR tube, but with a variable field applied during sample injection using a solenoid coil. The applied fields are written next to the corresponding data points.

in Fig. 6a was set up to transport water (^1H_2O) between a high-field (1.5 T) Halbach-array magnet for prepolarization [49] and an ultralow-field spectrometer where pulse-acquire NMR spectra were recorded at intervals of 2 s (2.5 μT; ^1H Larmor frequency ~100 Hz). Despite the fact that the ^1H spins are weakly polarized to the order of only 0.1 ppm, the water magnetization in this experiment begins many tens-of-thousands of times higher than the magnetization that would arise spontaneously at equilibrium in the detection field, and therefore the system can partially emulate the decay of a hyperpolarized sample including effects of nonadiabaticity. A commercially available atomic magnetometer (QuSpin zero-field magnetometer; QZFM2) was used to collect the low-frequency NMR signal from a 1 mL flow cell/reservoir located in the low-field region.

The polarizing magnet and the flow cell were around 30 cm away from one another and the fluidic connection was made by a 1-mm i.d. tube passing through ambient field. The flow rate of water through this system was measured to be 3 mL/min, which translated to a flow time of 3–4 s between the two field regions. Substantial loss of polarization due to relaxation may occur during this transport time. However, the transport was overall adiabatic and when the polarized water finally reached the detection cell its magnetization still remained far above the thermal equilibrium. Additionally, the magnetometer is highly sensitive, which led to signal-to-noise values of around 50 in the pulse-acquire NMR spectra.

We detected the adiabatic vs. nonadiabatic magnetization passage through metal by placing the needle VII in line between the polarizing and NMR-measurement fields (see Fig. 6a, inset). A 'guiding' solenoid coil several times longer than the needle's length was placed around the fluidic tubing and connected to a current supply so that the background magnetic field along the length of the needle could be controlled. The background field was turned on/off every 20 pulse-acquire measurements to observe the contrast effect on the magnetization reaching the flow cell. The idea is that when the solenoid is turned off, the polarized liquid passes through a region of field dominated by the magnetic field of the needle material, and if the transport through this field is nonadiabatic, it will lead to polarization and signal loss. If the solenoid provides a field that is significantly larger than that of the material, the overall transport will be adiabatic, leading to a recovery of the NMR signal. Indeed this type of contrast is observed: we compare Fig. 6b data obtained with no needle in line and Fig. 6c obtained with the needle VII. The clear modulation of the signal intensity in the latter case and its variation as a function of the field strength is evidence to state that strong nonadiabatic effects arise when the background field is below around 1 mT. It is unsurprising that the order of magnitude is the same as in the hyperpolarized ^{13}C experiments (Fig. 3(d)), given that the solution flow rates were similar and the same needle type (VII) was used, with the notable difference being the polarized nuclear spin species (^1H vs ^{13}C).

2.3. Magnetic field produced by a syringe needle

To better understand the reason why polarization is lost as solutions pass through a syringe needle, we have carried out additional measurements and simulations of the magnetic field produced by needle VII.

In Fig. 7 we show a 3-axis measurement of the magnetization of needle VII using three uniaxial vector magnetoresistance sensors (PNI Corp. RM3100 module) [50]. The syringe needle was placed adjacent to the x-axis sensor, close to the y- and z-axis sensors, and the magnetic field was measured at discrete intervals across one full revolution about the long axis (z). This is illustrated in the schematic in Fig. 7(a), and the results are shown in (b). We infer that the needle is magnetized transverse to the long axis due to the large, sinusoidal variation of the x and y field readings with rotation angle, and the field produced outside the needle at a distance of a few mm is on the order of tens of μT.

Using the known dimensions of needle VII (0.413 mm O.D., 0.21 mm I.D., 19 mm length), we generated a simulated map of the magnetic flux density using Comsol Multiphysics. The relative magnetic permeability of the material was set to 1 to approximately match that of stainless steel, and the remanent flux density of the needle was adjusted to 3 mT in the transverse ($+y$) direction to reproduce the measured field outside of the needed, via the process described above. The remaining volume was air with a relative magnetic permeability of 1. The maps are shown in Fig. 7(c), and exhibit several interesting features. First, there are noticeable field gradients at the ends of the needle, which differ depending on whether the end is sharp or blunt — these two cases apply to the head and tail end of the needle, respectively. Inside the needle the field is more homogeneous but much weaker in strength by approximately two orders of magnitude, due to

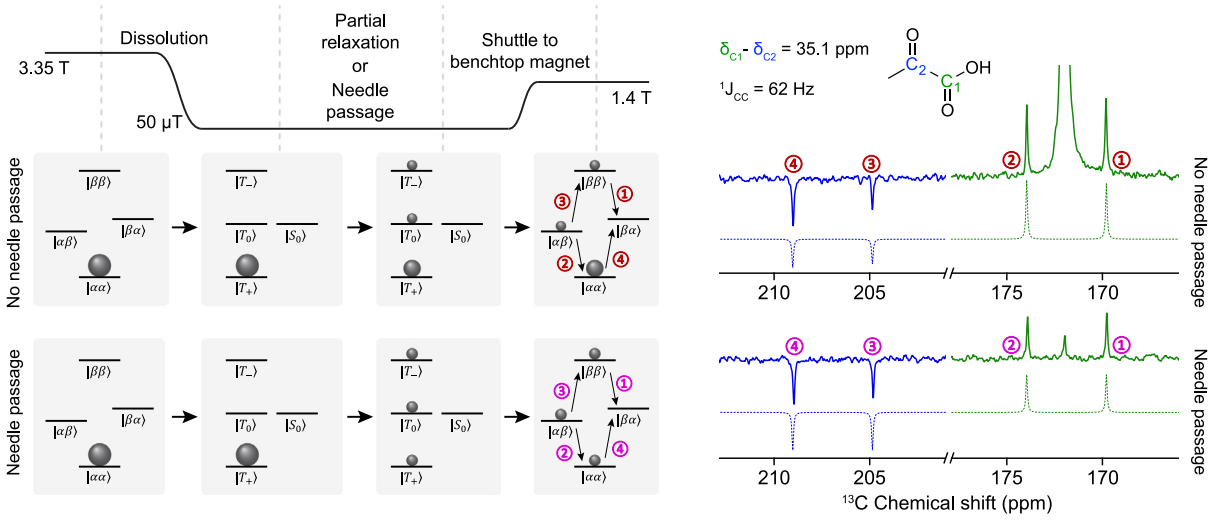

Fig. 4. Left: An (exaggerated) illustration of the ^{13}C spin state populations as they evolve during the course of the experiment. Passage through the needle leads to destruction of overall magnetization, illustrated by the equalization of the triplet state populations in low (50 μT) magnetic field. Without passage through a needle, T_1 relaxation anyway leads to partial redistribution of T_+ population to the other triplet states. The transitions that lead to observable NMR signals are labelled in red/pink. Right: Experimental data showing the ^1H-decoupled ^{13}C NMR signals from two samples acquired 12 s apart, where the first sample was passed through a plastic capillary (top) and the second was passed through a stainless steel syringe needle (bottom). Both spectra were acquired using a $\pi/2$ flip-angle pulse. Simulated spectra are shown (dashed lines) beneath the experimental spectra. These spectra were simulated by propagating a density operator of initial $\alpha\alpha$ spin order through the experimental process, using a $\pi/2$ pulse to redistribute the populations evenly within the triplet manifold to mimic passage through the needle, and filtering out coherences generated before the return to high field. In both simulations ^{13}C-^{13}C dipolar relaxation (which can induce relaxation within the triplet manifold) and relaxation from randomly fluctuating external fields was included. We observe good agreement between simulated peak amplitudes and experiment: this is particularly noticeable for the top spectrum in which peaks 3 and 4 are visibly different in amplitude than peaks 1 and 2. (For interpretation of the references to colour in this figure legend, the reader is referred to the web version of this article.)

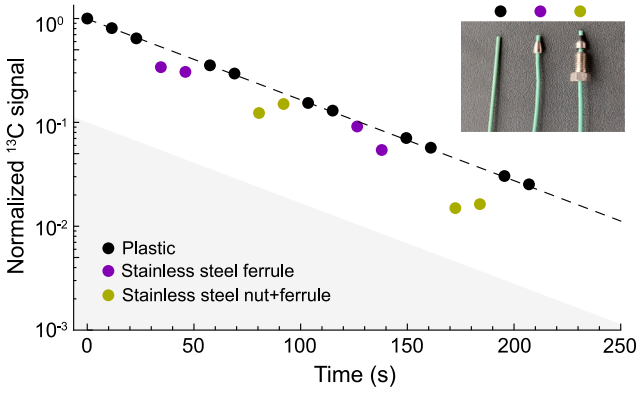

Fig. 5. Effect of stainless steel ferrules on the ^{13}C polarization. Data points represent the integrals of the [1-^{13}C]pyruvate ^{13}C NMR signal of the labelled C1 position, normalized to 1 for the first scan. The inset figure shows the capillary tubing, nut, and ferrules used for the injections. The dotted line represents an exponential decay function fit to the data, and the grey shaded region represents the area in which the ^{13}C integral is more than an order of magnitude lower than predicted from the control experiments.

geometric demagnetization. According to the theory presented in the Introduction, strong field gradients are main the cause of nonadiabatic polarization loss, therefore we believe that passage of solutions through the end/edge regions is the basis for the observed polarization losses. This is consistent with our observation that the angle of the needle in space does not correlate with polarization loss, since the field produced by the needle is large compared to the laboratory field. Although we cannot definitively say where the magnetization is lost without measurements where a guiding field is localized on specific parts of the needle, signal loss is dominated by the magnetization of the needle itself and not caused predominantly by the lower-field region within.

3. Discussion

Information on the internal stray field produced by small metallic components is important to describe the precise mechanism underlying the loss of nuclear spin polarization. Two factors are key: the inhomogeneity of the magnetic field, and rapid motion of the nuclei through the inhomogeneous field profile. We have not observed in any experiment that the magnetization is substantially preserved but reversed in sign, which suggests that the passage cannot be modelled as the spins moving nonadiabatically from the lab field into a homogeneous field within the metal component. This would behave like a 'pulse' on the spins of a given flip-angle, and the projection of the spin magnetization on the new quantization axis (z) may be either positive or negative, producing either an absorptive or emissive NMR signal.

The magnetization destruction effect can be suppressed by applying a magnetic field on the order of 0.1–10 mT around the metallic component to provide a strong-enough field to ensure adiabaticity of the spins during sample passage. The large field range we give (spanning two orders of magnitude) is based on the results obtained in Figs. 3(d) and 6(c), and is inherently broad since it depends on many experimental factors, such as the internal diameter and remanent magnetization of the needle, the nuclear spin species, and the solution flow rate. This can be done by constructing a magnetic tunnel along the sample transport path, [37] and in the case of in vivo imaging the intravenous injection can be carried out inside the MRI magnet [14]. From conversations with colleagues and from our own experience, we recognize that it is easy to unintentionally overlook the introduction of metallic parts into sample transport paths without due care. This is especially relevant for components such as nuts and ferrules, which are common in hyperpolarization apparatus for fluidic control, and have been shown to cause a partial loss of hyperpolarization that may go unnoticed.

Although 316 stainless steel is colloquially referred to as nonmagnetic, it can become weakly ferromagnetic during the manufacturing process. This property is not limited to steel; common aluminium alloys also exhibit a small degree of ferromagnetism that can affect NMR

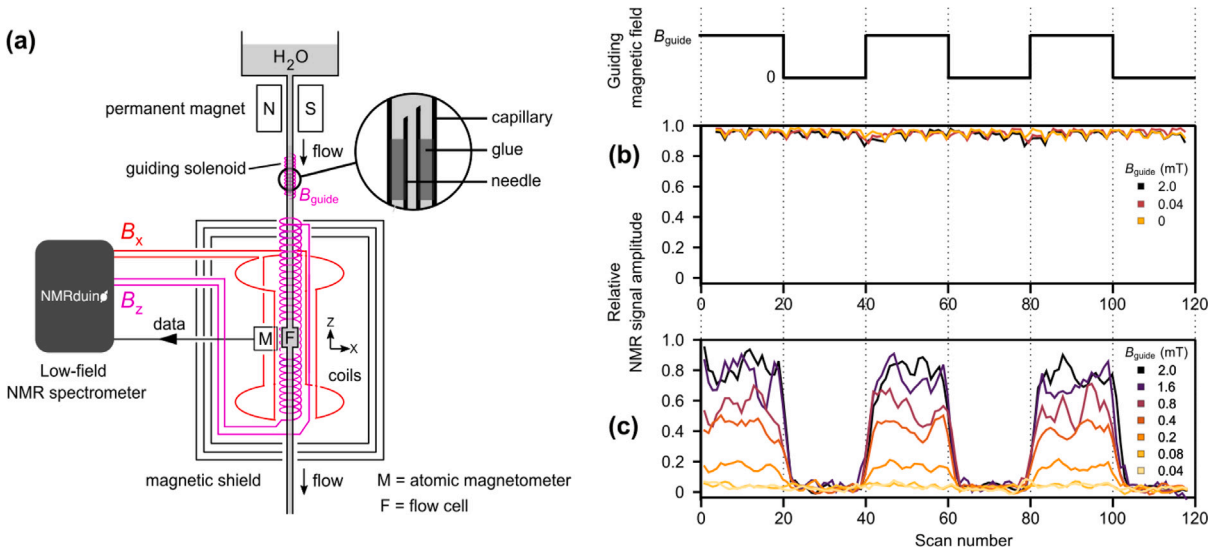

Fig. 6. Metal-induced polarization loss detected via low-field NMR. (a) system for μT NMR detection of H_2O with remote prepolarization. Liquid is flowed from the top reservoir under gravity, first through a permanent magnet (1.5 T) for thermal spin prepolarization and then the weaker field of a solenoid (0–2 mT) situated in the ambient field, and finally a magnetically shielded solenoid (2.5 μT) for pulse-acquire detection. The unshielded 'guiding' solenoid is toggled on/off every 20 pulse-acquire scans. Amplitudes of the precession signal (100 Hz for ^{1}H) detected in the flow cell are shown for equal flow rates with (b) no needle and (c) the needle VII (27G) placed inside the unshielded solenoid. Data points plotted in (c) are the moving average of 3 pulse-acquire scans.

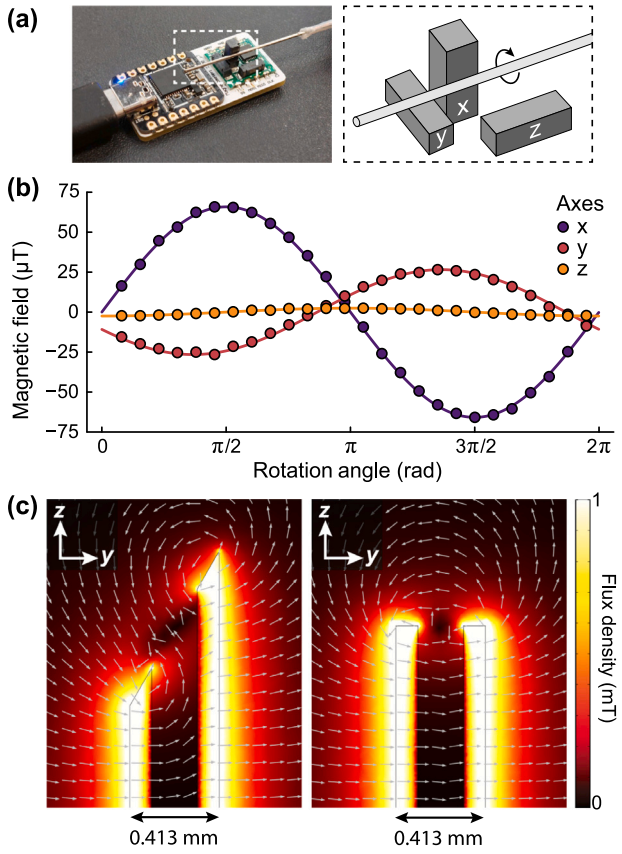

Fig. 7. (a) The experimental setup to measure the magnetic field outside syringe needle VII (27G, 3/4"). (b) The measured field in three axes during a full rotation of the needle. The three vector magnetometer probes are sensitive to fields along their long axes. (c) Simulations of the magnetic field flux density in and around the syringe needle. The plots show a transverse view of the sharp and blunt ends of a syringe needle, with the plane passing through the centre of the needle. The only magnetic field in the simulation was that of the needle itself, set to 3 mT in $+y$. The colour scale represents the absolute value of the magnetic flux density, while the arrows indicate the direction of the field at the base of the arrow.

measurements [51]. Steel is particularly susceptible to becoming ferromagnetic if it is cold-worked, which is typically how syringe needles are manufactured [52].

4. Conclusions

In this work we have studied the passage of magnetized solutions through metallic parts, and observed that in many cases the sample magnetization is diminished or lost due to nonadiabaticity of the passage. We have focused on solutions flowing through stainless steel hypodermic needles and capillary tubing supporting stainless steel nuts and ferrules, since these parts are commonplace in hyperpolarization equipment. The transport process can be made adiabatic by application of a magnetic field on the order of 0.1–10 mT around the metallic part, and the magnitude of this field is expected to depend on factors such as nuclear spin species, internal diameter and remanent magnetization of the metallic part, and solution flow rate.

This polarization-loss effect will be familiar to many researchers in the discipline, but commonly goes unnoticed in an applied setting. We hope our work will highlight this pitfall for scientists new to the field, and shed light on the phenomenon. We expect this effect to be especially relevant in the growing area of ultralow- and low-field MRI, [53–59] when hyperpolarized solutions are employed [60, 61]. These studies are typically carried out at between 5 to 60 mT field, meaning that even if the sample transport step is adiabatic, the field of the imaging magnet itself may not be high-enough to ensure adiabaticity of samples passing through syringe needles.

5. Methods

5.1. High-field experiments with hyperpolarized [1-^{13}C]pyruvate

To hyperpolarize [1-^{13}C]pyruvate, 24 μL of [1-^{13}C]pyruvic acid (Merck, Darmstadt, Germany) containing 15 mM trityl radical OX063 (GE Healthcare, Illinois, U.S.A.) and 1.5 mM gadoteric acid (Guerbet, Villepinte, France) was placed into a sample cup and inserted into a HyperSense commercial dissolution-DNP polarizer (Oxford Instruments Ltd., Oxford, U.K.) operating at 3.35 T magnetic field. This sample was cooled to 1.3 K, and irradiated with 100 mW microwaves at 94.115 GHz for approximately 40 min. The hyperpolarized frozen solid was then

Table 1
Summary of the seven metal syringe needles used in this work. Unless otherwise specified, needle VII was used for experiments.

Needle	Gauge	Length (in.)	Provider
I	21G	2	BD Microlance
II	20G	0.5	Darwin Microfluidics
III	19G	1	Henke Sass Wolf
IV	18G	1.5	BD Microlance
V	25G	5/8	BD Microlance
VI	25G	0.5	Darwin Microfluidics
VII	27G	3/4	BD Microlance

rapidly dissolved and flushed out of the polarizer by injecting 5.2 mL of heated phosphate buffered saline supplemented with 1% HEPES, 0.01% EDTA, 0.1% NaCl, and 0.2% NaOH (pH 12). This yielded a 5 mL solution of 80 mM [1-^{13}C]pyruvate at pH 7 and around 12.5%^{13}C polarization, which was collected in a plastic falcon tube. The resulting mixture was then further diluted by adding 10 mL MilliQ water, resulting in 15 mL of 27 mM [1-^{13}C]pyruvate solution. This dilution was performed to have enough sample to fill all the NMR tubes required for each experiment. The radicals (24 μM in our experiments) were not filtered because (i) the impact on T_1 is small, even at very low fields where the adiabatic condition fails to be met,[62] and (ii) to a large extent, relaxation and nonadiabaticity contributions to polarization loss are decoupled from one another.

The sample was extracted through a plastic capillary (1/16 inch O.D., 1/32 inch I.D., polyether ether ketone) into a 20 mL plastic syringe. At this point after extracting the sample from the polarizer it had not come into close contact with any metallic parts. The sample was then injected into 5 mm O.D. borosilicate NMR tubes through either the same plastic capillary (for control experiments), or a metal syringe needle, as described in the text. The sample injections were performed every T s (for Fig. 2 T = 10 s, for Fig. 3 T = 12 s), with 300–400 μL of hyperpolarized solution injected into each tube (a sufficient volume to completely fill the NMR coil to ensure quantitative measurements). After filling, each tube was immediately inserted into a 1.4 T benchtop NMR spectrometer (Pulsar, Oxford Instruments) and a ^{13}C NMR spectrum was recorded. The tube was then removed from the NMR magnet and discarded. In this way, the hyperpolarized [1-^{13}C]pyruvate solution was kept in the 20 mL plastic syringe, with a small aliquot ejected into a separate NMR tube every 10–12 s immediately prior to NMR signal acquisition. The acquisition parameters for all ^{13}C NMR measurements were an acquisition time of 3.2 s; 16 k data points; 90° flip-angle excitation pulse (15.5 μs).

5.2. Low-field experiments with magnetized water

Experimental data presented in Fig. 7(b) used a continuous-flow source of polarized water for high-throughput multi-sample measurement. Distilled water from a reservoir of several litres capacity drained continuously under gravity through a low-homogeneity 1.5 T magnet [49] allowing the ^{1}H spins to reach thermal equilibrium polarization on the order of 5 parts per million. The permanent magnet comprised a PEEK bore threaded on each end to accept standard 1/4–20 fluidic fittings. The polarized liquid subsequently flowed through a 1/16-inch inner-diameter PEEK capillary tube, passing from the stray field of the magnet, into the guiding field, and finally the ∼1 mL sample chamber located inside a compact four-layer magnetic shield (Magnetic Shields Limited, UK) for detection, see Fig. 7(a). Approximate dimensions of the shield were 16 cm height and 11 cm outer diameter.

The interior of the magnetic shield was fitted with a solenoid coil (∼7.5 mT/A) and a saddle coil (∼80 μT/A), centred upon the flow cell to produce magnetic fields along z and x axes, respectively. Current applied to the solenoid was kept constant at 2.5 μT and controlled using a 10 mA low-noise DC driver (Twinleaf LLC model CSB-10), while the saddle coil was switched on/off for each NMR measurement with a dc pulse of duration 500 μs and current 150 mA to rotate ^{1}H spins by a flip angle of 90°. For a more detailed description of the electronic components used to generate the pulses, see past work [63]. Finally, the guiding field was powered using a standard laboratory power supply (HAMEG instruments HM8040-3).

The ^{1}H spin precession signals following each x-coil pulse were detected by a compact, commercially available atomic magnetometer (QuSpin LLC, QZFM2) positioned next to the flow cell with its sensitive axis along the y direction. The timing of the pulses and data acquisition was controlled by an open-source low-field NMR spectrometer console (NMRduino [64]).

5.3. Syringe needles used in this work

See Table 1.

CRediT authorship contribution statement

James Eills: Conceptualization, Formal analysis, Investigation, Visualization, Writing – original draft. **Marc Azagra:** Data curation, Investigation, Visualization, Writing – review & editing. **David Gómez-Cabeza:** Investigation, Visualization, Writing – review & editing. **Michael C.D. Tayler:** Conceptualization, Funding acquisition, Investigation, Methodology, Visualization, Writing – original draft. **Irene Marco-Rius:** Conceptualization, Funding acquisition, Project administration, Resources, Supervision, Writing – review & editing.

Declaration of competing interest

The authors declare that they have no known competing financial interests or personal relationships that could have appeared to influence the work reported in this paper.

Data availability

Data will be made available on request.

Acknowledgements

This work has received funding from: The European Union's Horizon 2020 research and innovation program (GA-863037); The European Union MSCA European Postdoctoral Fellowships (GA-101063517); the Spanish grants with reference PID2020-117859RA-I00 funded by MCIN/ AEI/ 10.13039/ 501100011033 (NARMYD), RYC2020-029099-I and RYC2022-035450-I funded by MCIN/ AEI10.13039/ 501100011033 and by "ESF Investing in your future", PLEC2022-009256 funded by MCIN/ AEI/ 10.13039/ 501100011033 and by the "European Union NextGenerationEU/PRTR", and PID2021-126059OA-I00 funded by MCIN/AEI/10.13039/501100011033 (MARICHAS); The Generalitat de Catalunya "Severo Ochoa" Center of Excellence (CEX2019-000910-S); Fundació Privada Cellex; Fundació Mir-Puig; The BIST (Barcelona Institute of Science and Technology)-"la Caixa" Banking Foundation Chemical Biology programme; J.E. was supported in part by a Fundació Bosch Aymerich (FBA) fellowship through BIST.

References

[1] J.H. Ardenkjær-Larsen, B. Fridlund, A. Gram, G. Hansson, L. Hansson, M.H. Lerche, R. Servin, M. Thaning, K. Golman, Increase in signal-to-noise ratio of >10,000 times in liquid-state NMR, Proc. Natl. Acad. Sci. 100 (18) (2003) 10158–10163.
[2] S.J. Elliott, Q. Stern, M. Ceillier, T. El Daraï, S.F. Cousin, O. Cala, S. Jannin, Practical dissolution dynamic nuclear polarization, Prog. Nucl. Magn. Reson. Spectrosc. 126 (2021) 59–100.
[3] G. Zhang, C. Hilty, Applications of dissolution dynamic nuclear polarization in chemistry and biochemistry, Magn. Reson. Chem. 56 (7) (2018) 566–582.
[4] S. Jannin, J.-N. Dumez, P. Giraudeau, D. Kurzbach, Application and methodology of dissolution dynamic nuclear polarization in physical, chemical and biological contexts, J. Magn. Reson. 305 (2019) 41–50.

[5] P. Niedbalski, A. Kiswandhi, C. Parish, Q. Wang, F. Khashami, L. Lumata, NMR spectroscopy unchained: attaining the highest signal enhancements in dissolution dynamic nuclear polarization, J. Phys. Chem. Lett. 9 (18) (2018) 5481–5489.

[6] T.C. Eisenschmid, R.U. Kirss, P.P. Deutsch, S.I. Hommeltoft, R. Eisenberg, J. Bargon, R.G. Lawler, A.L. Balch, Para hydrogen induced polarization in hydrogenation reactions, J. Am. Chem. Soc. 109 (26) (1987) 8089–8091.

[7] C.R. Bowers, D.P. Weitekamp, Parahydrogen and synthesis allow dramatically enhanced nuclear alignment, J. Am. Chem. Soc. 109 (18) (1987) 5541–5542.

[8] S.B. Duckett, R.E. Mewis, Application of para hydrogen induced polarization techniques in NMR spectroscopy and imaging, Acc. Chem. Res. 45 (8) (2012) 1247–1257.

[9] J.-B. Hövener, A.N. Pravdivtsev, B. Kidd, C.R. Bowers, S. Glöggler, K.V. Kovtunov, M. Plaumann, R. Katz-Brull, K. Buckenmaier, A. Jerschow, et al., Parahydrogen-based hyperpolarization for biomedicine, Angew. Chem. Int. Ed. 57 (35) (2018) 11140–11162.

[10] A.B. Schmidt, C.R. Bowers, K. Buckenmaier, E.Y. Chekmenev, H. de Maissin, J. Eills, F. Ellermann, S. Glöggler, J.W. Gordon, S. Knecht, et al., Instrumentation for hydrogenative parahydrogen-based hyperpolarization techniques, Anal. Chem. 94 (1) (2022) 479–502.

[11] J. Eills, D. Budker, S. Cavagnero, E.Y. Chekmenev, S.J. Elliott, S. Jannin, A. Lesage, J. Matysik, T. Meersmann, T. Prisner, J.A. Reimer, H. Yang, I.V. Koptyug, Spin hyperpolarization in modern magnetic resonance, Chem. Rev. 123 (2023) 1417–1551, PMID: 36701528.

[12] S.J. Nelson, J. Kurhanewicz, D.B. Vigneron, P.E. Larson, A.L. Harzstark, M. Ferrone, M. Van Criekinge, J.W. Chang, R. Bok, I. Park, et al., Metabolic imaging of patients with prostate cancer using hyperpolarized [1-^{13}C] pyruvate, Sci. Transl. Med. 5 (198) (2013) 198ra108.

[13] F.A. Gallagher, M.I. Kettunen, D.-E. Hu, P.R. Jensen, M. Karlsson, A. Gisselsson, S.K. Nelson, T.H. Witney, S.E. Bohndiek, G. Hansson, et al., Production of hyperpolarized [1, 4-$^{13}c_2$] malate from [1, 4-$^{13}c_2$] fumarate is a marker of cell necrosis and treatment response in tumors, Proc. Natl. Acad. Sci. USA 106 (47) (2009) 19801–19806.

[14] I. Marco-Rius, C. von Morze, R. Sriram, P. Cao, G.-Y. Chang, E. Milshteyn, R.A. Bok, M.A. Ohliger, D. Pearce, J. Kurhanewicz, et al., Monitoring acute metabolic changes in the liver and kidneys induced by fructose and glucose using hyperpolarized [2-^{13}C] dihydroxyacetone, Magn. Reson. Med. 77 (1) (2017) 65–73.

[15] E. Cavallari, C. Carrera, M. Sorge, G. Bonne, A. Muchir, S. Aime, F. Reineri, The ^{13}C hyperpolarized pyruvate generated by ParaHydrogen detects the response of the heart to altered metabolism in real time, Sci. Rep. 8 (1) (2018) 1–9.

[16] M. Gierse, L. Nagel, M. Keim, S. Lucas, T. Speidel, T. Lobmeyer, G. Winter, F. Josten, S. Karaali, M. Fellermann, et al., Parahydrogen-polarized fumarate for preclinical in vivo metabolic magnetic resonance imaging, J. Am. Chem. Soc. (2023).

[17] G.L. Olsen, O. Szekely, B. Mateos, P. Kadeřávek, F. Ferrage, R. Konrat, R. Pierattelli, I.C. Felli, G. Bodenhausen, D. Kurzbach, et al., Sensitivity-enhanced three-dimensional and carbon-detected two-dimensional NMR of proteins using hyperpolarized water, J. Biomol. NMR 74 (2–3) (2020) 161–171.

[18] C. Hilty, D. Kurzbach, L. Frydman, Hyperpolarized water as universal sensitivity booster in biomolecular NMR, Nat. Protoc. 17 (7) (2022) 1621–1657.

[19] R. Mandal, P. Pham, C. Hilty, Characterization of protein–ligand interactions by SABRE, Chem. Sci. 12 (39) (2021) 12950–12958.

[20] R. Mandal, P. Pham, C. Hilty, Screening of protein–ligand binding using a SABRE hyperpolarized reporter, Anal. Chem. 94 (32) (2022) 11375–11381.

[21] B. Gizatullin, C. Mattea, S. Stapf, Field-cycling NMR and DNP–A friendship with benefits, J. Magn. Reson. 322 (2021) 106851.

[22] Y. Lee, G.S. Heo, H. Zeng, K.L. Wooley, C. Hilty, Detection of living anionic species in polymerization reactions using hyperpolarized NMR, J. Am. Chem. Soc. 135 (12) (2013) 4636–4639.

[23] E.V. Pokochueva, D.B. Burueva, O.G. Salnikov, I.V. Koptyug, Heterogeneous catalysis and parahydrogen-induced polarization, ChemPhysChem 22 (14) (2021) 1421–1440.

[24] W. Wang, Q. Wang, J. Xu, F. Deng, Understanding heterogeneous catalytic hydrogenation by parahydrogen-induced polarization NMR spectroscopy, ACS Catal. 13 (2023) 3501–3519.

[25] A. Guthertz, M. Leutzsch, L.M. Wolf, P. Gupta, S.M. Rummelt, R. Goddard, C. Farès, W. Thiel, A. Fürstner, Half-sandwich ruthenium carbene complexes link trans-hydrogenation and gem-hydrogenation of internal alkynes, J. Am. Chem. Soc. 140 (8) (2018) 3156–3169.

[26] W. Jiang, Q. Peng, H. Sun, Q. Zhang, C. Huang, S. Cao, X. Wang, Z. Chen, Determining the enantioselectivity of asymmetric hydrogenation through parahydrogen-induced hyperpolarization, J. Chem. Phys. 155 (16) (2021) 161101.

[27] I. Marco-Rius, A. Comment, In vivo hyperpolarized ^{13}CMRS and MRI applications, in: Handbook of High Field Dynamic Nuclear Polarization, John Wiley & Sons, 2019, p. 405.

[28] B. Melton, V. Pollak, T. Mayes, B.L. Willis, Condition for sudden passage in the Earth's-field NMR technique, J. Magn. Reson. A 117 (2) (1995) 164–170.

[29] B.A. Rodin, J. Eills, R. Picazo-Frutos, K.F. Sheberstov, D. Budker, K.L. Ivanov, Constant-adiabaticity ultralow magnetic field manipulations of parahydrogen-induced polarization: application to an AA'X spin system, Phys. Chem. Chem. Phys. 23 (2021) 7125–7134.

[30] B. Meier, J.-N. Dumez, G. Stevanato, J.T. Hill-Cousins, S.S. Roy, P. Håkansson, S. Mamone, R.C. Brown, G. Pileio, M.H. Levitt, Long-lived nuclear spin states in methyl groups and quantum-rotor-induced polarization, J. Am. Chem. Soc. 135 (50) (2013) 18746–18749.

[31] A.S. Kiryutin, B.A. Rodin, A.V. Yurkovskaya, K.L. Ivanov, D. Kurzbach, S. Jannin, D. Guarin, D. Abergel, G. Bodenhausen, Transport of hyperpolarized samples in dissolution-DNP experiments, Phys. Chem. Chem. Phys. 21 (25) (2019) 13696–13705.

[32] M. Ceillier, O. Cala, T. El Daraï, S.F. Cousin, Q. Stern, S. Guibert, S.J. Elliott, A. Bornet, B. Vuichoud, J. Milani, et al., An automated system for fast transfer and injection of hyperpolarized solutions, J. Magn. Reson. Open 8 (2021) 100017.

[33] T. Harris, O. Szekely, L. Frydman, On the potential of hyperpolarized water in biomolecular NMR studies, J. Phys. Chem. B 118 (12) (2014) 3281–3290.

[34] P. Pham, R. Mandal, C. Qi, C. Hilty, Interfacing liquid state hyperpolarization methods with NMR instrumentation, J. Magn. Reson. Open 10 (2022) 100052.

[35] M. Krajewski, P. Wespi, J. Busch, L. Wissmann, G. Kwiatkowski, J. Steinhauser, M. Batel, M. Ernst, S. Kozerke, A multisample dissolution dynamic nuclear polarization system for serial injections in small animals, Magn. Reson. Med. 77 (2) (2017) 904–910.

[36] E. Cavallari, C. Carrera, S. Aime, F. Reineri, Studies to enhance the hyperpolarization level in PHIP-SAH-produced C13-pyruvate, J. Magn. Reson. 289 (2018) 12–17.

[37] J. Milani, B. Vuichoud, A. Bornet, P. Miéville, R. Mottier, S. Jannin, G. Bodenhausen, A magnetic tunnel to shelter hyperpolarized fluids, Rev. Sci. Instrum. 86 (2) (2015) 024101.

[38] F. Jähnig, G. Kwiatkowski, M. Ernst, Conceptual and instrumental progress in dissolution DNP, J. Magn. Reson. 264 (2016) 22–29.

[39] A.C. Pinon, A. Capozzi, J.H. Ardenkjær-Larsen, Hyperpolarized water through dissolution dynamic nuclear polarization with UV-generated radicals, Commun. Chem. 3 (1) (2020) 57.

[40] K. Kouřil, H. Kouřilová, S. Bartram, M.H. Levitt, B. Meier, Scalable dissolution-dynamic nuclear polarization with rapid transfer of a polarized solid, Nat. Commun. 10 (1) (2019) 1733.

[41] N. Chattergoon, F. Martínez-Santiesteban, W. Handler, J.H. Ardenkjær-Larsen, T. Scholl, Field dependence of T1 for hyperpolarized [1-13C] pyruvate, Contrast Media Mol. Imaging 8 (1) (2013) 57–62.

[42] B. Gizatullin, C. Mattea, S. Stapf, Hyperpolarization by DNP and molecular dynamics: Eliminating the radical contribution in NMR relaxation studies, J. Phys. Chem. B 123 (46) (2019) 9963–9970.

[43] H. Shang, T. Skloss, C. von Morze, L. Carvajal, M.V. Criekinge, E. Milshteyn, P.E.Z. Larson, R.E. Hurd, D.B. Vigneron, Handheld electromagnet carrier for transfer of hyperpolarized carbon-13 samples, Magn. Reson. Med. 75 (2) (2015) 917–922.

[44] M.C.D. Tayler, I. Marco-Rius, M.I. Kettunen, K.M. Brindle, M.H. Levitt, G. Pileio, Direct enhancement of nuclear singlet order by dynamic nuclear polarization, J. Am. Chem. Soc. 134 (18) (2012) 7668–7671.

[45] I. Marco-Rius, M.C.D. Tayler, M.I. Kettunen, T.J. Larkin, K.N. Timm, E.M. Serrao, T.B. Rodrigues, G. Pileio, J.H. Ardenkjaer-Larsen, M.H. Levitt, et al., Hyperpolarized singlet lifetimes of pyruvate in human blood and in the mouse, NMR Biomed. 26 (12) (2013) 1696–1704.

[46] W. Iali, S.S. Roy, B.J. Tickner, F. Ahwal, A.J. Kennerley, S.B. Duckett, Hyperpolarising pyruvate through signal amplification by reversible exchange (SABRE), Angew. Chem. 131 (30) (2019) 10377–10381.

[47] M.H. Levitt, Singlet nuclear magnetic resonance, Ann. Rev. Phys. Chem. 63 (2012) 89–105.

[48] G. Pileio, Singlet NMR methodology in two-spin-1/2 systems, Prog. Nucl. Magn. Reson. Spectrosc. 98 (2017) 1–19.

[49] M.C.D. Tayler, D. Sakellariou, Low-cost, pseudo-Halbach dipole magnets for NMR, J. Magn. Reson. 277 (2017) 143–148.

[50] https://github.com/MichaelTayler/RM3100-XIAO. (Accessed 30 August 2023).

[51] M.C.D. Tayler, J. Ward-Williams, L.F. Gladden, Ultralow-field nuclear magnetic resonance of liquids confined in ferromagnetic and paramagnetic materials, Appl. Phys. Lett. 115 (7) (2019).

[52] https://www.industrialheating.com/articles/89463-hypodermic-the-holey-needle. (Accessed 30 August 2023).

[53] C.P. Bidinosti, J. Choukeife, G. Tastevin, P.-J. Nacher, A. Vignaud, MRI of the lung using hyperpolarized 3 He at very low magnetic field (3 mT), Magn. Reson. Mater. Phys. Biol. Med. 16 (2004) 255–258.

[54] T. O'Reilly, W. Teeuwisse, A. Webb, Three-dimensional MRI in a homogenous 27 cm diameter bore Halbach array magnet, J. Magn. Reson. 307 (2019) 106578.

[55] L.M. Broche, P.J. Ross, G.R. Davies, M.-J. MacLeod, D.J. Lurie, A whole-body fast field-cycling scanner for clinical molecular imaging studies, Sci. Rep. 9 (1) (2019) 1–11.

[56] Y. He, W. He, L. Tan, F. Chen, F. Meng, H. Feng, Z. Xu, Use of 2.1 MHz MRI scanner for brain imaging and its preliminary results in stroke, J. Magn. Reson. 319 (2020) 106829.
[57] M. Sarracanie, N. Salameh, Low-field MRI: how low can we go? A fresh view on an old debate, Front. Phys. 8 (2020) 172.
[58] Y. Liu, A.T. Leong, Y. Zhao, L. Xiao, H.K. Mak, A.C.O. Tsang, G.K. Lau, G.K. Leung, E.X. Wu, A low-cost and shielding-free ultra-low-field brain MRI scanner, Nat. Commun. 12 (1) (2021) 7238.
[59] T.C. Arnold, C.W. Freeman, B. Litt, J.M. Stein, Low-field MRI: Clinical promise and challenges, J. Magn. Reson. Imaging 57 (1) (2023) 25–44.
[60] K. Buckenmaier, M. Rudolph, P. Fehling, T. Steffen, C. Back, R. Bernard, R. Pohmann, J. Bernarding, R. Kleiner, D. Koelle, et al., Mutual benefit achieved by combining ultralow-field magnetic resonance and hyperpolarizing techniques, Rev. Sci. Instrum. 89 (12) (2018) 125103.
[61] S.-J. Lee, K. Jeong, J.H. Shim, H.J. Lee, S. Min, H. Chae, S.K. Namgoong, K. Kim, SQUID-based ultralow-field MRI of a hyperpolarized material using signal amplification by reversible exchange, Sci. Rep. 9 (1) (2019) 12422.
[62] K. Mouloudakis, S. Bodenstedt, M. Azagra, M.W. Mitchell, I. Marco-Rius, M.C.D. Tayler, Real-time polarimetry of hyperpolarized ^{13}C nuclear spins using an atomic magnetometer, J. Phys. Chem. Lett. 14 (5) (2023) 1192–1197.
[63] S. Bodenstedt, M.W. Mitchell, M.C.D. Tayler, Meridional composite pulses for low-field magnetic resonance, Phys. Rev. A 106 (3) (2022).
[64] M.C.D. Tayler, S. Bodenstedt, NMRduino: a modular, open-source, low-field magnetic resonance platform, J. Magn. Reson. (2024) submitted for publication.